Supplementary Information for
Thickness model for viscous impinging liquid sheets

The basic assumption of this theory is that the velocity within the jet is uniform. As the jet length increases, the velocity distribution evolves from a parabolic to a uniform profile before impinging. The evolution of velocity profile is verified by direct numerical simulations. Simulations are based on the open-source code OpenFOAM (https://openfoam.com), and it is solved using the interIsoFoam solver. The simulation of a single jet is performed to verify the evolution of the velocity profile within the jet. The effectiveness of this approach has been validated in our previous numerical research[1]. Figure 1(a) illustrates the geometric model used in the numerical simulation with the corresponding boundary conditions. The cylindrical region represents the pipe through which the jet flows, with a diameter of 50 μm and a length of 500 μm, ensuring the complete development of the jet. Figure 1(b) shows the mesh configuration of the geometric model, with a background mesh size of 20 μm. Local mesh refinements are applied near the wall, resulting in a smallest mesh size of 2 μm to ensure accurate capture of the jet's internal velocity. Figure 1(c) depicts the simulated single jet, where L denotes the distance from the cylinder pipe outlet to the given section. The magnified jet cross-section illustrates the velocity distribution.

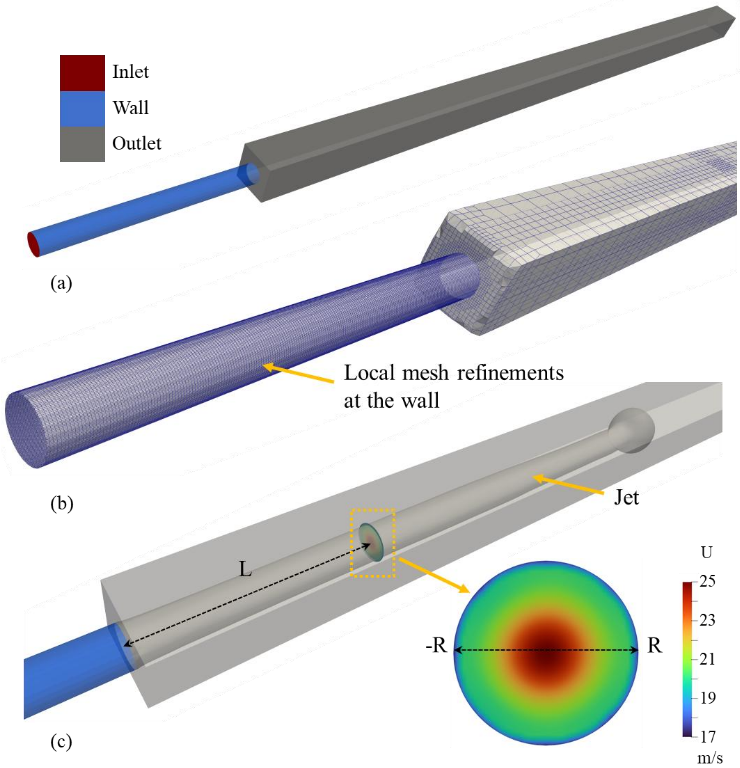

Fig.1 (a) The geometry model for numerical simulations with boundary conditions. (b) Mesh refinements for geometry model showing local mesh refinements at the wall. (c) The simulation of a single jet indicating extraction of a velocity profile.

Figure 2 illustrates the evolution of the jet velocity profile with distance under three different viscosity conditions. After the jet exits the pipe, all cases exhibit a transition from a parabolic velocity profile to a uniform velocity profile. For the low-viscosity condition, the velocity profile becomes uniform at L=1000 μm, as shown in Fig. 2(a). For the high-viscosity condition, the velocity profile becomes uniform at L=500 μm, as shown in Fig. 2(c).

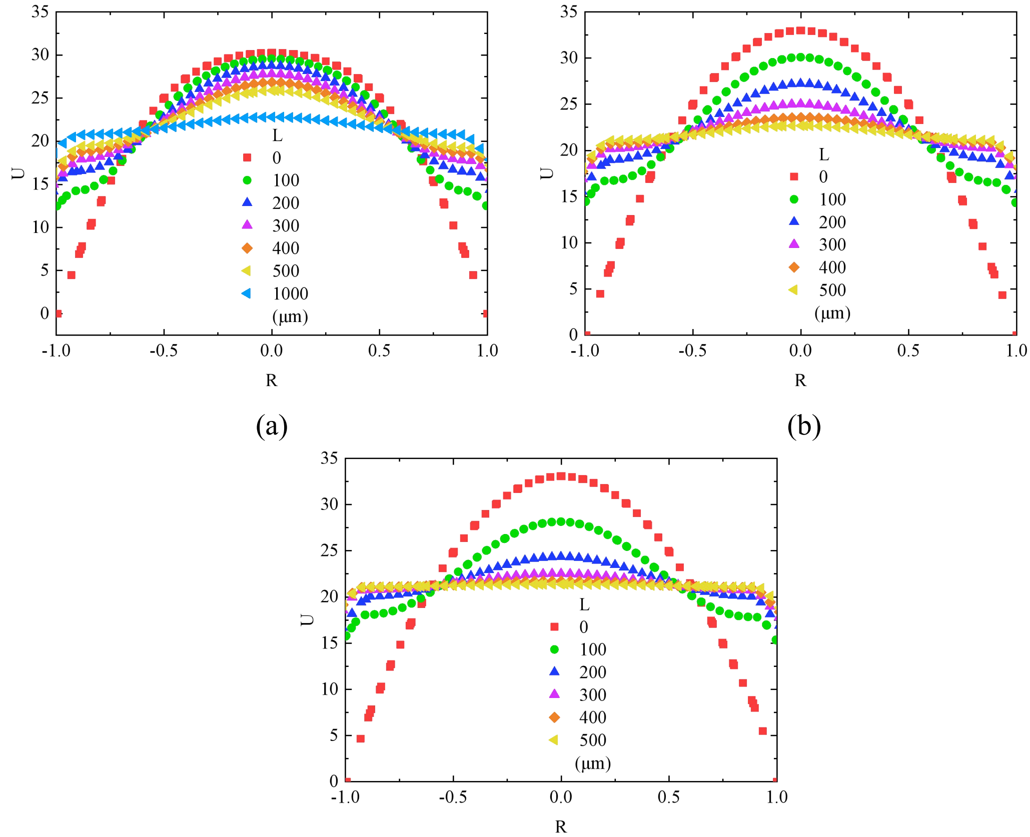

(a) (b)

(c)

Fig.2 Evolution of jet velocity profile with distance at different viscosities, with (a) 1.97 cst, (b) 4.85 cst, and (c) 8.25 cst.

We experimentally set the pre-impingement jet length to over 1 mm to ensure a uniform jet velocity profile. Therefore, the jet velocity can be represented by a single variable u_j. Assuming a steady flow of the ultra-thin liquid sheet, the Navier-Stokes equations are simplified to:

$$u_r \frac{\partial u_r}{\partial r} + \frac{u_\phi}{r}\frac{\partial u_r}{\partial \phi} - \frac{u_\phi^2}{r} = \nu\left(\Delta \mathrm{u_r} - \frac{2}{r^2}\frac{\partial u_\phi}{\partial \phi} - \frac{u_r}{r^2}\right) \tag{1}$$

$$u_r \frac{\partial u_\phi}{\partial r} + \frac{u_\phi}{r}\frac{\partial u_\phi}{\partial \phi} + \frac{u_r u_\phi}{r} = \nu\left(\Delta u_\phi + \frac{2}{r^2}\frac{\partial u_r}{\partial \phi} - \frac{u_\phi}{r^2}\right) \tag{2}$$

We consider a 2-D sheet velocity: $\vec{u}_s = (u + u_r^{(1)})\vec{e}_r + u_\phi^{(1)}\vec{e}_\phi$, substituting into (1) and get $u\dfrac{\partial u}{\partial r} = 0$, i.e. $u(r,\phi) = u(\phi)$. Therefore, we can solve the following system of equations: (3) and (4), which are simplified from (1) and (2), respectively; and (5), which represents the conservation of flow at a specific point in the sheet:

$$u\frac{\partial u_r^{(1)}}{\partial r} + \frac{u_\phi^{(1)}}{r}\frac{\partial u}{\partial \phi} = \nu\left(\frac{1}{r^2}\frac{\partial^2 u}{\partial \phi^2} - \frac{u}{r^2}\right) \tag{3}$$

$$u\frac{\partial u_\phi^{(1)}}{\partial r} + \frac{u u_\phi^{(1)}}{r} = \frac{2\nu}{r^2}\frac{\partial u}{\partial \phi} \tag{4}$$

$$\frac{1}{r}\frac{\partial[(u+u_r^{(1)})hr]}{\partial r}+\frac{1}{r}\frac{\partial(u_\phi^{(1)}h)}{\partial\phi}=0 \tag{5}$$

The equation (4) yields:

$$u_\phi^{(1)}=\frac{2\nu}{u}\frac{\partial u}{r\partial\phi}\ln\frac{r}{R} \tag{6}$$

Where R is the the boundary condition that u_ϕ is equal to 0. We can add a perturbation term to: $hr=q_j{}^2\sin\theta[1+\delta(r,\phi)]$, and substituting into (5):

$$\frac{\partial u_r^{(1)}}{\partial r}+u\frac{\partial\delta}{\partial r}+\frac{\partial}{\partial\phi}\left(\frac{u_\phi^{(1)}}{r}\right)+2\frac{\partial q_j(\phi)}{q_j(\phi)\partial\phi}\frac{u_\phi^{(1)}}{r}=0 \tag{7}$$

Combining (3) and (7):

$$\frac{\partial\delta}{\partial r}=\frac{\nu}{u^2}\left(\frac{u}{r^2}-\frac{1}{r^2}\frac{\partial^2u}{\partial\phi^2}\right)+\frac{u_\phi^{(1)}}{u^2r}\frac{\partial u}{\partial\phi}-\frac{\partial u_\phi^{(1)}}{ur\partial\phi}-2\frac{\partial q_j(\phi)}{q_j(\phi)\partial\phi}\frac{u_\phi^{(1)}}{ur} \tag{8}$$

The result is derived by substituting equation (6) into equation (8):

$$\frac{\partial\delta}{\partial r}=\frac{\nu}{u^2r^2}\left[u-\frac{\partial^2u}{\partial\phi^2}+2\frac{\partial u}{\partial\phi}\frac{\partial q_j}{q_j\partial\phi}+\left(\frac{2}{u}\left(\frac{\partial u}{\partial\phi}\right)^2-2u\frac{\partial\left(\frac{1}{u}\frac{\partial u}{\partial\phi}\right)}{\partial\phi}-4\frac{\partial u}{\partial\phi}\frac{\partial q_j}{q_j\partial\phi}\right)\ln\frac{r}{q_jR}\right] \tag{9}$$

Separating the variables in equation (9):

$$\frac{\partial\delta}{\partial r}=a\left[\phi,U(\phi)\right]\frac{\nu}{Q}\left[1+f(r,\phi)\right] \tag{10}$$

Here $Q=\pi R_j^2u_j^2$ is the jet flow rate, $U(\phi)=u/u_j$ is the dimensionless velocity distribution, and $a\left[\phi,U(\phi)\right]$, $f(r,\phi)$ are:

$$a(\phi)=\frac{\pi R_j^2}{U^2r_0^2}\{U-\frac{\partial^2U}{\partial\phi^2}+2\frac{\partial U}{\partial\phi}\frac{\partial q_j}{q_j\partial\phi}+[\frac{2}{U}(\frac{\partial U}{\partial\phi})^2-2U\frac{\partial}{\partial\phi}(\frac{\partial U}{U\partial\phi})-4\frac{\partial U}{\partial\phi}\frac{\partial q_j}{q_j\partial\phi}]\ln\frac{r_1}{q_jR}\} \tag{11}$$

$$f(r,\phi)=\frac{(U-\frac{\partial^2U}{\partial\phi^2}+2\frac{\partial U}{\partial\phi}\frac{\partial q_j}{q_j\partial\phi})(\frac{1}{r^2}-\frac{1}{r_0^2})+[\frac{2}{U}(\frac{\partial U}{\partial\phi})^2-2U\frac{\partial}{\partial\phi}(\frac{\partial U}{U\partial\phi})-4\frac{\partial U}{\partial\phi}\frac{\partial q_j}{q_j\partial\phi}](\frac{\ln\frac{r}{q_jR}}{r^2}-\frac{\ln\frac{r_1}{q_jR}}{r_0^2})}{\frac{1}{r_0^2}\{U-\frac{\partial^2U}{\partial\phi^2}+2\frac{\partial U}{\partial\phi}\frac{\partial q_j}{q_j\partial\phi}+[\frac{2}{U}(\frac{\partial U}{\partial\phi})^2-2U\frac{\partial}{\partial\phi}(\frac{\partial U}{U\partial\phi})-4\frac{\partial U}{\partial\phi}\frac{\partial q_j}{q_j\partial\phi}]\ln\frac{r_1}{q_jR}\}} \tag{12}$$

Where R and r_0 and r_1 are undetermined parameters. Nevertheless, within the physical scenario we are discussing, we can reasonably expect $f(r,\phi)\ll 1$. Expanding the thickness to the viscosity: $h=h_0+\nu\times h_1+\cdots$, and based on dimensional analysis, We can express: $h_1=u_j^{-1}\times\zeta(R_j/r,\phi)$, and ζ is a dimensionless function. It is physically reasonable to assume that ζ is bounded as $R_j\to 0$, so we can expand ζ given that $R_j\ll r$: $\zeta=\zeta_0+\zeta_1R_j/r+\cdots$, and get:

$$h=h_0+\frac{\nu}{u_j}\left[\zeta_0(\phi)+\zeta_1(\phi)\times\frac{R_j}{r}+\zeta_2(\phi)\times\frac{R_j^2}{r^2}+\zeta_3(\phi)\times\frac{R_j^3}{r^3}+\cdots\right] \tag{13}$$

Comparing with equation (10), we see that:

$$a(\phi)=\frac{\pi\zeta_0(\phi)}{q_j^2(\phi)\sin\theta} \tag{14}$$

$$f(r,\phi)=-\frac{\zeta_2(\phi)}{\zeta_0(\phi)}\frac{R_j^2}{r^2}-\frac{2\zeta_3(\phi)}{\zeta_0(\phi)}\frac{R_j^3}{r^3}+\cdots \tag{15}$$

Therefore, $f\left(r,\phi\right)\ll 1$ when we consider $R_j \ll r$. This indicats that equation (15) exhibits weak dependence on r, and (10) can be expressed as:

$$\frac{\partial\delta}{\partial r}=a\left[\phi,U\left(\phi\right)\right]\frac{\nu}{Q} \tag{16}$$

This is a universal conclusion, requiring only that u be a function of ϕ, irrespective of its specific form. In principle, it applies to liquid sheets under arbitrary impinging angles θ.

A specific solution to $a\left[\phi,U\left(\phi\right)\right]$ necessitates determining the explicit form of u, which could be dependent on impinging angle θ. Assuming a flat velocity distribution at $\phi=0$ ($\frac{\partial^2 u}{\partial\phi^2}=\frac{\partial^4 u}{\partial\phi^4}=0$), and truncating the series $u=u_j\sum_k a_k\cos\left(k\phi\right)$ to fourth order:

$$u(\phi)=u_j\left[\gamma+\alpha\cos\phi+\epsilon\cos 2\phi-\left(\frac{5\alpha}{21}+\frac{16}{21}\right)\cos 3\phi+\left(\frac{\alpha}{14}+\frac{5}{28}\right)\cos 4\phi\right] \tag{17}$$

Equation (17) should still be universal; however, ensuring mass, momentum, and energy conservation when determining its coefficients requires specifying the value of b, potentially dependent on θ. In the case of $b=0.69R_j\cot\theta$ in our experiments, we obtain:

$$u/u_j=0.147+0.408\cos\phi+0.879\cos 2\phi-0.767\cos 3\phi+0.186\cos 4\phi \tag{18}$$

This is effective within an azimuth range of ±50 degrees, which is sufficient because the leaf-like shape of the liquid sheet concentrates most of its area within this angular range. The subsequent analysis, which is clearly outlined in the article, will not be reiterated in this document.

The sheet length mentioned in Fig. 4(h) in the article is defined as Fig.3 below. We also provide a table of the composition and physical properties of the mixtures used in the experiment.

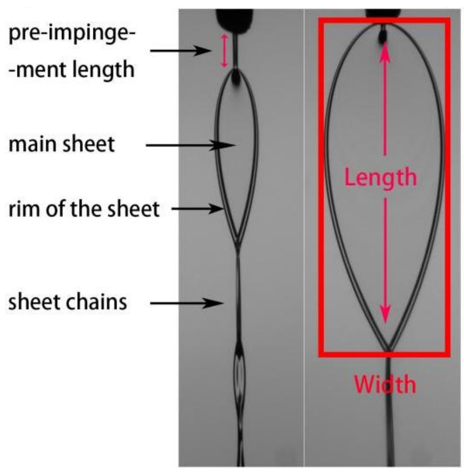

Fig.3 Photograph of the generated liquid sheet and definitions of key terminology.

Table.1 Physical properties of the mixtures used in the experiment.

Mass Fraction			Refractive-index	Density	Dynamic viscosity	Kinematic viscosity	Surface tension
Water	Ethanol	Glycerol		g/cm^3	mPa·s	mm^2/s	mN/m
0	60	40	1.405	0.943	6.08	6.45	25.05
0	55.5	44.5	1.413	0.971	7.81	8.04	25.49
0	50	50	1.415	0.988	10.9	11.04	25.99
40	20	40	1.4	1.063	5.46	5.14	33.67
20	40	40	1.402	0.998	6.71	6.72	28.13
25	25	50	1.412	1.065	10.04	9.43	31.07
16.7	33.3	50	1.397	1.001	10.46	10.45	28.87
50	0	50	1.399	1.131	4.85	4.29	65.33
100	0	0	1.332	1	1.01	1.01	71.78
0	100	0	1.361	0.778	1.17	1.50	21.86
60	40	0	1.373	0.962	2.51	2.61	29.35
30	70	0	1.362	0.851	1.99	2.34	25.62
35	0	65	1.438	1.212	11.19	9.24	65.33
40	0	60	1.424	1.184	8.25	6.97	65.36
60	0	40	1.391	1.12	3.03	2.70	66.03
71.5	0	28.5	1.379	1.098	1.97	1.79	68.87
0	42	58	1.432	1.043	18.76	17.99	26.86
0	70	30	1.41	0.933	3.37	3.61	24.03
15	55	30	1.406	0.968	4.31	4.45	26.15
30	40	30	1.405	1.013	4.53	4.47	28.36
45	25	30	1.398	1.049	4.15	3.96	32.25
50	10	40	1.414	1.134	4.46	3.93	42.01
30	30	40	1.412	1.054	5.89	5.59	30.43
10	50	40	1.414	0.993	6.17	6.21	26.5
40	10	50	1.42	1.141	7.12	6.24	40.69
33.3	16.7	50	1.411	1.092	8.29	7.59	34.92
45	5	50	1.411	1.14	5.81	5.10	49.27
37.5	2.5	60	1.428	1.183	9.05	7.65	55
30	10	60	1.426	1.146	12.48	10.89	39.43
25	15	60	1.434	1.144	15.06	13.16	35.76
57	5	38	1.396	1.114	3.2	2.87	50.86
31	0	69	1.442	1.218	14.15	11.62	64.86
0	0	100	1.473	1.261	953.5	756.15	62.17
90	10	0	1.352	1.015	1.27	1.25	47.35
75	25	0	1.361	0.982	1.85	1.88	34.82

References

[1] Wu E, Wang B, Chong W K, et al. Turbulent atomisation of impinging jets under rising backpressure[J]. Journal of Fluid Mechanics, 2025, 1003: A15.